

Mechanistic Investigation of Green Fluorescent Protein Acquiring Energy for Emitting Light: A Theoretical Study

Shuangqi Pi, Deping Hu,* and Ya-Jun Liu*



Cite This: *J. Phys. Chem. B* 2025, 129, 2925–2933



Read Online

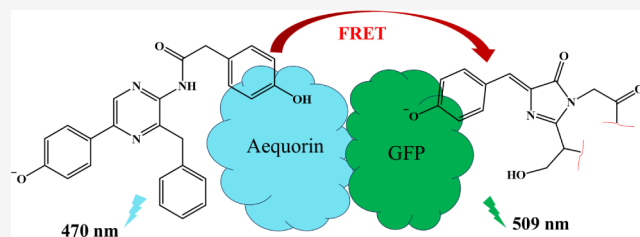
ACCESS |

Metrics & More

Article Recommendations

Supporting Information

ABSTRACT: Green fluorescent protein (GFP) is famous for noninvasively observing the internal biological processes of cells and organisms, revolutionizing the field of cell biology. GFP was first discovered in jellyfish *Aequorea victoria* (AV). The GFP bioluminescence (BL) in AV can be divided into three stages: the first singlet excited state coelenteramide (S_1 -CTD) is formed in aequorin; GFP acquires energy from S_1 -CTD via an energy transfer (ET) process; and GFP emits green light. The first and final stages have been well studied, whereas the detailed mechanism of the second stage remains unclear, with only sporadic experimental evidence. The purpose of this study is to clarify how GFP acquires energy before emitting green light in AV. Through protein–protein docking, molecular dynamics simulations, and combined quantum mechanics and molecular mechanics calculations, we demonstrate that the ET process occurs via the Förster resonance energy transfer (FRET) mechanism. The calculated FRET rate is faster than the radiative and nonradiative decay ones of S_1 -CTD, which means the ET process can occur efficiently. Additionally, the calculated fluorescence quantum yield explains the experimentally observed BL enhancement after the ET. This is the first theoretical report on the ET mechanism in BL. This study not only clearly interprets how GFP acquires energy for emitting light but also helps to understand the ET mechanism in other bioluminescent systems and sheds new light on bioluminescence resonance energy transfer.



The purpose of this study is to clarify how GFP acquires energy before emitting green light in AV. Through protein–protein docking, molecular dynamics simulations, and combined quantum mechanics and molecular mechanics calculations, we demonstrate that the ET process occurs via the Förster resonance energy transfer (FRET) mechanism. The calculated FRET rate is faster than the radiative and nonradiative decay ones of S_1 -CTD, which means the ET process can occur efficiently. Additionally, the calculated fluorescence quantum yield explains the experimentally observed BL enhancement after the ET. This is the first theoretical report on the ET mechanism in BL. This study not only clearly interprets how GFP acquires energy for emitting light but also helps to understand the ET mechanism in other bioluminescent systems and sheds new light on bioluminescence resonance energy transfer.

1. INTRODUCTION

Over the past decades, the development and application of green fluorescent protein (GFP) have revolutionized the field of cell biology.¹ Therefore, the Nobel Prize in 2008 was awarded for the discovery and applications of GFP.² GFP is widely used as a fluorescent marker to visualize dynamic biological processes, making it essential in areas such as developmental biology,^{3,4} disease treatment,^{5,6} and biosensing.⁷ GFP was first discovered by Shimomura et al. during their study of the bioluminescence (BL) mechanism of the jellyfish *Aequorea victoria* (AV).⁸ After years of research, researchers believe that there are two sets of BL systems in AV, and the BL process can be divided into three stages as shown in Scheme 1.⁹ In the first stage, in aequorin, with the addition of Ca^{2+} , 2-hydroperoxycoelenterazine (2-hydroperoxy-CTZ) converts to CTZ dioxetanone (CDO) and the latter rapidly dissociates to generate the first singlet excited state coelenteramide (S_1 -CTD).¹⁰ In the second stage, the energy transfer (ET) process occurs from S_1 -CTD to GFP.^{11,12} In the final stage, GFP emits green light of a 509 nm wavelength.¹² Extensive research focused on the final stage of GFP luminescence, uncovering the maturation process mechanism of GFP,^{13,14} identifying the chemical form of the chromophore (CRO) in GFP,^{14,15} simulating the fluctuations and dynamics of GFP,^{16–18} and mutating the CRO and surrounding residues to modify the light emission.^{19–22} The first stage has been also clearly evidenced by experimental and theoretical studies.^{23–25}

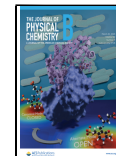
Suppose there was no ET process in the second stage, S_1 -CTD would decay to S_0 -CTD and emit blue light at the wavelength of 470 nm,^{8,9} similar to most marine bioluminescent organisms. So, the second stage is vital for GFP emitting light. However, in the second stage, the detailed process and underlying mechanism of how energy transfers from S_1 -CTD to GFP still remain unclear, except for limited experimental evidence confirming the occurrence of the ET process.^{11,12} Investigating the ET mechanism and details experimentally is challenging, as the ET process is very complex, which involves not only donor–acceptor interactions but also protein–protein interactions. Additionally, it is a dynamic process *in vivo*, making it difficult to directly obtain the structure of the protein–protein complex using both X-ray diffraction and nuclear magnetic resonance (NMR) spectroscopy.²⁶ The experimental studies also found that the BL intensity increases (about 1.2-fold enhancement) after the ET process occurs.¹² The fluorescence quantum yield in the first stage is 0.20 in basic DMSO,²⁷ but 0.72 for GFP.¹² The

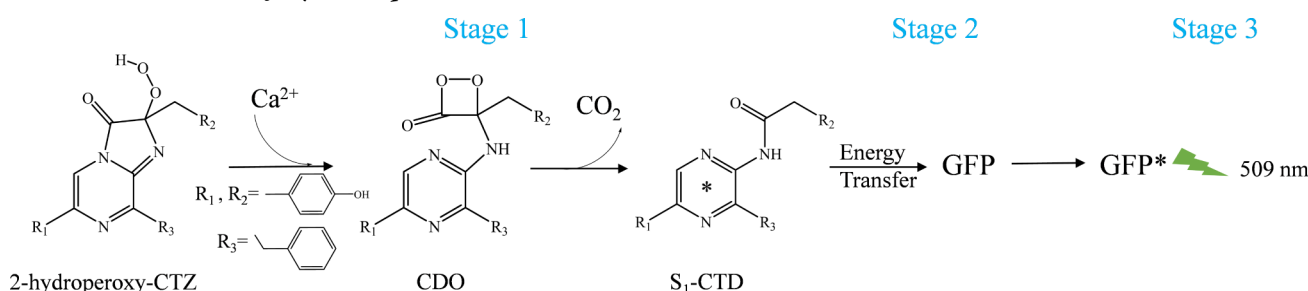
Received: December 9, 2024

Revised: February 26, 2025

Accepted: March 3, 2025

Published: March 7, 2025



Scheme 1. BL Process of Jellyfish *Aequorea victoria*

phenomenon of increasing BL intensity has never been clearly interpreted. In the present study, we comprehensively applied the protein–protein docking, molecular dynamics (MD) simulations, and combined quantum mechanics and molecular mechanics (QM/MM) to study the specific ET processes in AV BL. This study makes up the completeness of the entire BL process of GFP in AV and is of great importance to deeply understand the ET mechanism in bioluminescence resonance energy transfer (BRET).²⁸ BRET can shift the BL to the near-infrared region, which greatly improves the BL imaging depth and resolution in living organisms.^{29,30} Furthermore, ET plays a crucial role in the process of photosynthesis and the development of luminescent materials.^{31,32}

2. MATERIALS AND METHODS

2.1. Computational Models. As shown in Scheme 1, the first stage takes place in AV aequorin, so the X-ray crystallographic structure of AV aequorin from the PDB data bank (PDB: 1EJ3) was selected.³³ The 2-hydroperoxy-CTZ is bound in the cavity of AV aequorin as a substrate. Experimental and theoretical studies have confirmed that the phenolate anion form of $\text{S}_1\text{-CTD}$ ($\text{S}_1\text{-CTD}^-$) in AV aequorin is the actual bioluminophore, capable of emitting blue light at 470 nm, see Figure 1a.^{34,35} Therefore, we modified 2-hydroperoxy-CTZ as CTD^- for later calculations. Yue have

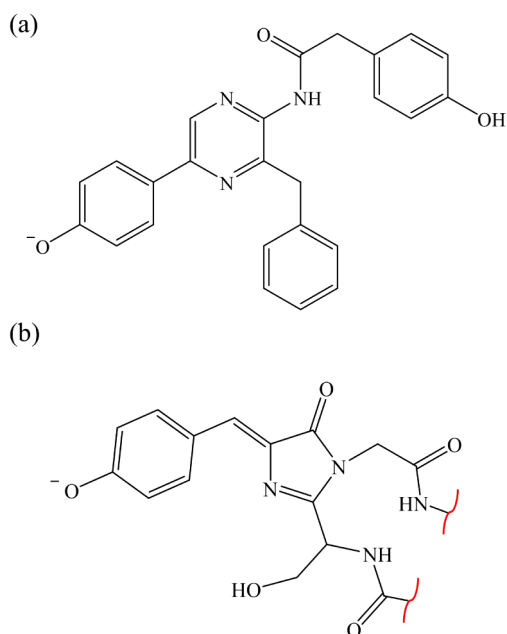


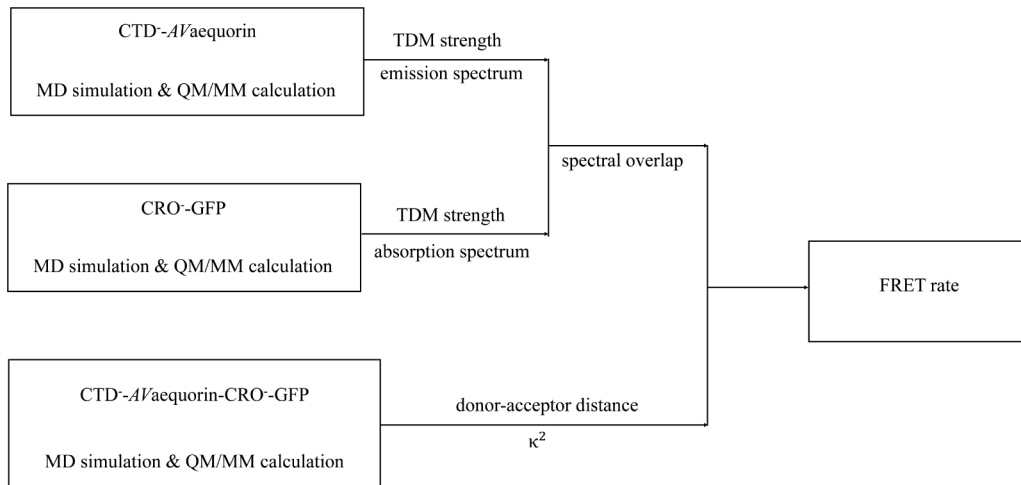
Figure 1. Structures of the phenolic anion form of CTD [CTD⁻] (a) and the anion form of CRO [CRO⁻] (b).

already studied the reaction mechanism of the first stage, so further investigation is unnecessary here.²⁵ Then, the energy transfers from $\text{S}_1\text{-CTD}$ in AV aequorin to GFP. Based on previous studies, the energy acceptor is the CRO within GFP, rather than the entire GFP.¹² The CRO is formed by cyclization, dehydration, and oxidation of residues Ser65, Tyr66, and Gly67.¹³ In the final stage, experimental and theoretical studies have confirmed that the anionic form of $\text{S}_1\text{-CRO}$ ($\text{S}_1\text{-CRO}^-$) is the actual bioluminophore responsible for 509 nm green light, see Figure 1b.^{36–38} Studies also found that both neutral and anionic forms of CRO exist in GFP, and the molar ratio of neutral to anionic form is 6:1.³⁹ However, the absorption of neutral CRO (peak at 395 nm)³⁸ is out of resonance conditions with the emission of $\text{S}_1\text{-CTD}^-$ in AV aequorin. We also calculated the spectrum of neutral CRO, and the results (see Figure S1) indicate a very small spectral overlap between the absorption of neutral CRO in GFP and the emission of $\text{S}_1\text{-CTD}^-$ in AV aequorin, which is consistent with the experimental observations. Therefore, in subsequent discussions and calculations, we will focus exclusively on the anionic form of CRO. The X-ray crystallographic structure of GFP from the PDB data bank (PDB: 1GFL) was selected for later calculations.⁴⁰

After determining the computational models of ET from $\text{S}_1\text{-CTD}^-$ in 1EJ3 to $\text{S}_1\text{-CRO}^-$ in 1GFL, we first conducted protein–protein docking with AV aequorin and GFP. In the obtained AV aequorin-GFP complex, we calculated the interface area and analyzed its properties to assess the stability of the complex. Then, by conducting MD simulations and QM/MM calculations on the AV aequorin-GFP complex, we calculated the ET rate and efficiency. The relevant calculation details involved are as follows.

2.2. Protein–Protein Docking and MD Simulations. After the computational models were set up, all water molecules were removed from AV aequorin and GFP before protein–protein docking. Cluspro 2.0 server^{41,42} was employed for protein–protein docking to obtain the AV aequorin–GFP complex. The highest-scoring protein–protein complex was selected for later calculations.

The systems were solvated in an octahedron box of TIP3P waters⁴³ extending up to a minimum cutoff of 10 Å from the protein surface. Sodium ions were added to neutralize the total charge of the system. We performed 30 ns MD simulations for AV aequorin and GFP, respectively. For the AV aequorin–GFP complex obtained through docking, we performed a longer 200 ns MD simulation to confirm its stable existence. To shorten the main text, the details of MD simulations and further explanations are provided in the Supporting Information. The RMS deviation analyses are presented in Figure S2. All MD simulations were performed at a constant temperature of 300 K and a pressure of 1.0 atm via the Amber 16 package.⁴⁴

Scheme 2. Workflow of the FRET Rate Calculations

2.3. QM/MM Calculation. QM/MM calculations were used to calculate the vertical absorption wavelength (λ_A , nm) and the vertical emission wavelength (λ_F , nm) of CTD^- and CRO^- . For AV aequorin, the QM regions were selected as CTD^- . For GFP, the QM regions were selected as CRO^- . The N–C and C–C single bonds were cut off (red line in Figure 1) and the H link atoms were added. The rest of the systems, excluding the QM region, were selected as the MM region. For the QM region, the geometry optimizations of S_0 and S_1 -states were calculated at TD ω B97X-D3/def2-SVP level.^{45,46} In the MM region, the side chains of residues and water molecules within 5 Å of the QM region were allowed to relax during the geometry optimizations. Geometry optimizations were performed in the ChemShell^{47–49} computational chemistry environment. ORCA⁵⁰ and DL_POLY⁵¹ were employed for the QM and MM calculations, respectively. The electrostatic embedding (EE) scheme was employed to consider the polarization effect of the MM region on the QM region.

Based on the optimized geometries of the QM region and the background point charges of the MM region, the complete active space second-order perturbation theory (CASPT2) method⁵² with the ANO-RCC-VDZP basis set was employed to calculate the oscillator strength (f), transition dipole moments (TDM), λ_A and λ_F of the QM region (CTD^- and CRO^-). The active spaces of 14-in-13 and 16-in-14 were chosen for CTD^- and CRO^- , respectively, in CASPT2 calculations (see Figures S3 and S4). The Molcas 8.2 program⁵³ was used for CASPT2 calculations, and the background point charges of the MM region were added to the electrostatic potential fitting (ESPF) module to simulate the polarization of the MM region on the QM region. To consider the effect of protein fluctuation on the absorption and emission spectra,⁵⁴ we selected three snapshots at 23, 24, and 25 ns in the production region from the MD trajectories and used the geometry of these snapshots as the initial geometry of the QM/MM calculations to calculate λ_A and λ_F (see Tables S1 and S2).

When studying the ET process, substrates CTD^- and CRO^- , as well as the protein environment AV aequorin–GFP were all taken into consideration. CTD^- and CRO^- were involved in the QM region, while the rest of the atoms of AV aequorin–GFP were in the MM region. In the MM region, the side chains of residues and the water molecules within 5 Å of

the QM region were allowed to relax during the optimizations. The geometries of CTD^- and CRO^- complex at the S_1 state were optimized at TD ω B97X-D3/def2-SVP level by ORCA and DL_POLY in the ChemShell package. The EE scheme was employed to consider the polarization effect of the MM region on the QM region.

2.4. Förster Resonance Energy Transfer (FRET) Calculations. ET occurs between an energy donor at the excited state (D^*) and an energy acceptor at the ground state (A). In our system, $S_1\text{-}\text{CTD}^-$ is the donor and $S_0\text{-}\text{CRO}^-$ is the acceptor. Through ET, $S_0\text{-}\text{CTD}^-$ and $S_1\text{-}\text{CRO}^-$ can be obtained. The rate of FRET (k_{ET}) can be calculated by formula 1

$$k_{\text{ET}} = (\hbar^2 c)^{-1} |V_{\text{DA}}|^2 J \quad (1)$$

where \hbar is the reduced Planck constant and c is the light speed. V_{DA} is the electrostatic interaction between the initial state $D^*\text{A}$ and the final state DA^* . Under the point dipole approximation and taking the effect of the solvent environment into account, V_{DA} can be written as

$$\begin{aligned} |V_{\text{DA}}|^2 &= \left| \frac{1}{4\pi\epsilon_0\eta^2 r^3} \left[(\vec{\mu}_D \cdot \vec{\mu}_A) - \frac{3}{r^2} (\vec{\mu}_D \cdot \vec{r})(\vec{\mu}_A \cdot \vec{r}) \right] \right|^2 \\ &= \frac{1}{(4\pi\epsilon_0)^2} \frac{\kappa^2}{\eta^4 r^6} |\mu_D|^2 |\mu_A|^2 \end{aligned} \quad (2)$$

where $\vec{\mu}_{D(A)}$ represents the TDM vector of the donor (acceptor). \vec{r} represents the distance vector between the donor and acceptor. ϵ_0 is the vacuum permittivity. η is the refractive index of the protein environment. It has been suggested that the appropriate value for the refractive index of amino acids within protein is 1.6.^{56–58} The orientation factor, κ^2 can be expressed by formula 3.

$$\kappa^2 = (\cos \theta_T - 3 \cos \theta_D \cos \theta_A)^2 \quad (3)$$

θ_T is the angle between $\vec{\mu}_D$ and $\vec{\mu}_A$. θ_D is the angle between $\vec{\mu}_D$ and \vec{r} . θ_A is the angle between $\vec{\mu}_D$ and \vec{r} . J in formula 1 represents the overlap integral of the normalized emission spectrum [$F_D(\tilde{\nu})$] of the donor and the normalized absorption

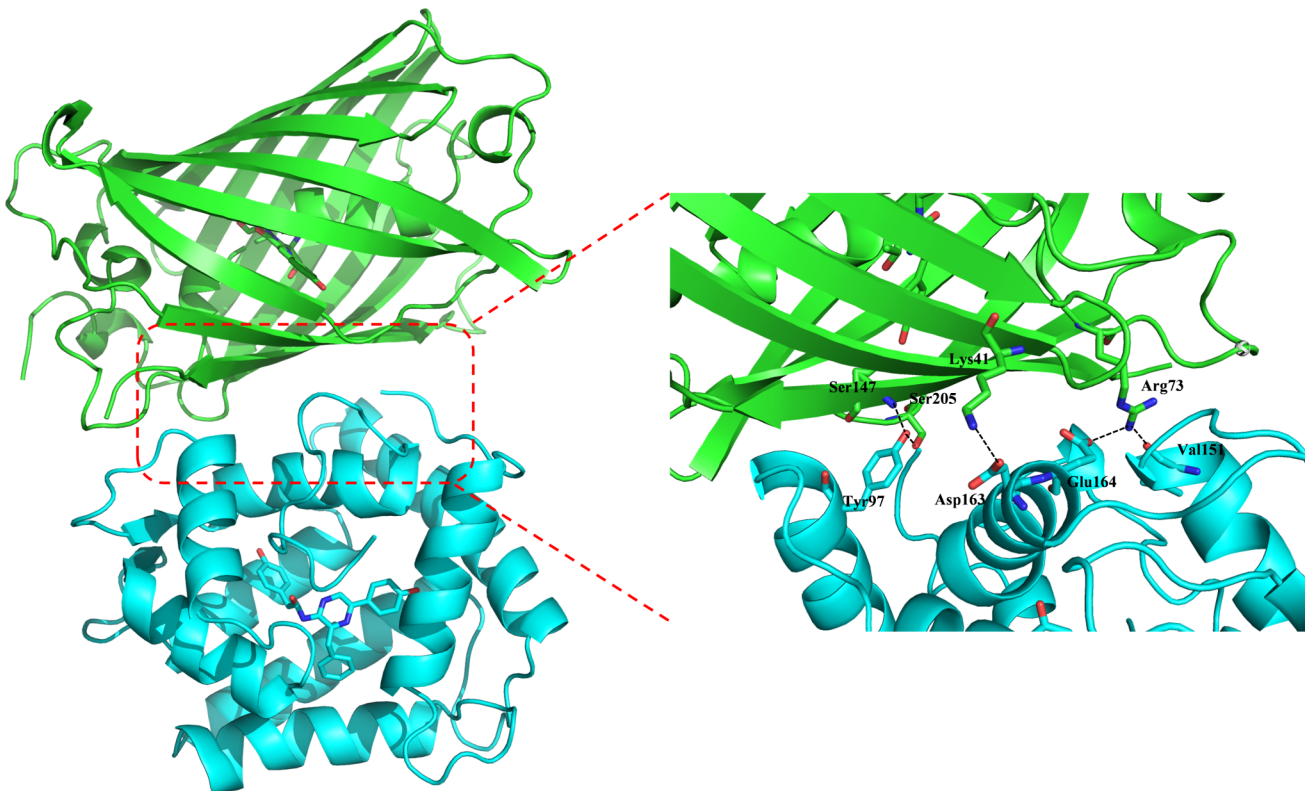


Figure 2. Views of amino acid residues that form hydrogen bonds in the AV aequorin–GFP interface. The cyan-colored protein represents AV aequorin while the green-colored protein represents GFP, respectively.

spectrum [$A_A(\tilde{\nu})$] of the acceptor in area and can be calculated by formula 4.

$$J = \int_0^\infty F_D(\tilde{\nu}) A_A(\tilde{\nu}) d\tilde{\nu} \quad (4)$$

$F_D(\tilde{\nu})$ and $A_A(\tilde{\nu})$ can be obtained from the emission spectrum [$f_D(\tilde{\nu})$] and absorption spectrum [$\epsilon_A(\tilde{\nu})$] by formulas 5 and 6. $\tilde{\nu}$ is the wavenumber in cm^{-1} .

$$F_D(\tilde{\nu}) = \frac{f_D(\tilde{\nu})/\tilde{\nu}^3}{\int_0^\infty d(\tilde{\nu}) f_D(\tilde{\nu})/\tilde{\nu}^3} \quad (5)$$

$$A_A(\tilde{\nu}) = \frac{\epsilon_A(\tilde{\nu})/\tilde{\nu}}{\int_0^\infty d(\tilde{\nu}) \epsilon_A(\tilde{\nu})/\tilde{\nu}} \quad (6)$$

$|\mu_D|^2$ ($|\mu_A|^2$) can be obtained from the QM/MM calculations. The details of formula derivations are presented in Supporting Information. Based on the introduction above, our calculation process is shown in Scheme 2.

2.5. Spectrum, Radiative, and Nonradiative Decay Process Simulations. The absorption spectrum of the acceptor (CRO^-) and the emission spectrum of the donor (CTD^-) were simulated, along with calculations for the radiative (k_R) and nonradiative (k_{NR}) decay rates of both donor and acceptor at 300 K. These calculations were carried out using the thermal vibration correlation function (TVCF) formalism in the MOMAP package,^{59–62} see Supporting Information for details. The quantum yield of the radiative process was calculated using formula 7.

$$\Phi = \frac{k_R}{k_R + k_{NR}} \quad (7)$$

In TVCF calculations, it is essential to obtain the geometries and vibrational frequencies of S_0^- and $S_1\text{-CTD}^-$ in AV aequorin, as well as those of S_0^- and $S_1\text{-CRO}^-$ in GFP. Additionally, the adiabatic energies, TDMs, and nonadiabatic couplings (NACs) between the S_0 and S_1 states are also required. In our calculations, the adiabatic energies of CTD^- and CRO^- between the S_0 and S_1 states as well as the TDMs were calculated at the CASPT2/ANO-RCC-VDZP/MM level as shown in Section 2.3. The vibrational frequencies of CTD^- and CRO^- at the S_0 and S_1 states were calculated at the TD $\omega\text{B97X-D3/def2-SVP/MM}$ level by using the ORCA and DL_POLY programs in ChemShell. The NACs of CTD^- and CRO^- between S_0 and S_1 states were calculated at the $\omega\text{B97X-D/def2-SVP/MM}$ level with the Gaussian 16 package by adding the background point charges of the MM region to simulate electrostatic coupling between the QM and MM regions.

3. RESULTS AND DISCUSSION

3.1. Analysis of the AV Aequorin–GFP Complex Interface. To investigate the mechanism of the ET process between CTD^- and CRO^- , we first analyzed the interface properties of the AV aequorin–GFP complex on the PDBePISA server. The total area of AV aequorin–GFP interface is about 2060 \AA^2 , which is large enough for a protein–protein complex.⁶³ The interfacing area is shown in Figure S5 (the gray part). For AV aequorin–GFP, the analysis results shown in Figure 2 indicate that hydrogen bonds can be formed between Tyr97, Val151, Asp163, and Glu164 in AV aequorin and Lys41, Lys73, Ser147, and Ser205 in GFP. The surface electrostatic potential of AV aequorin and GFP was calculated by PDB2PQR and evaluated in the adaptivePois-

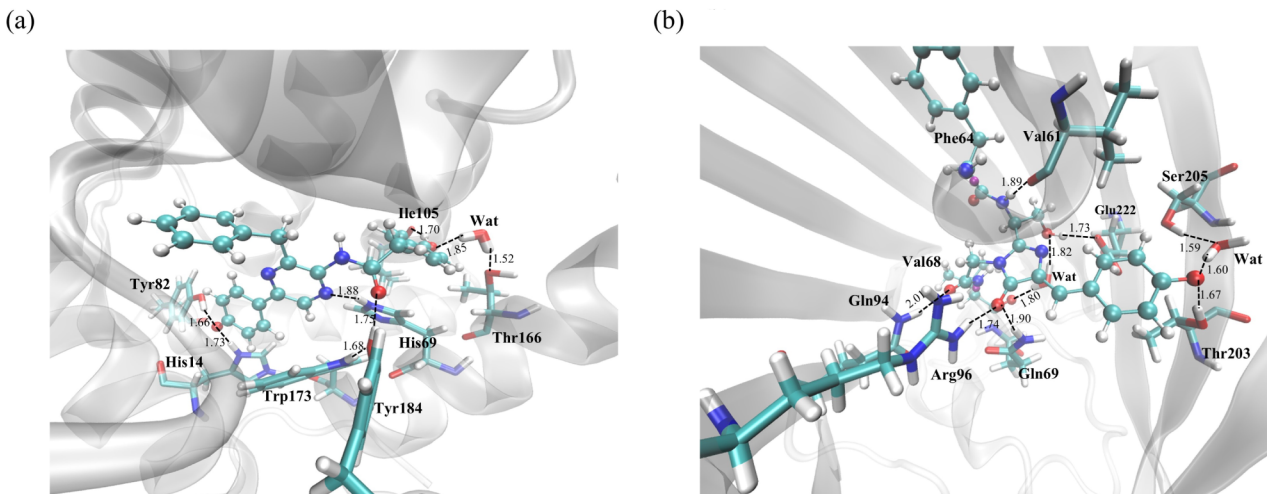


Figure 3. Optimized geometries and hydrogen bonding networks of S_1 -CTD $^-$ in (a) AV aequorin as well as S_0 -CRO $^-$ in (b) GFP calculated at the TD ω B97X-D3/def2-SVP/MM level. The purple atom in (b) is the H link atom. The unit of the hydrogen bond length is Å.

son–Boltzmann solver (APBS). The calculation results are listed in Figure S6. For AV aequorin–GFP, the interfacing residues in AV aequorin are mostly negatively charged, while the interfacing residues of GFP are mostly positively charged. In the interfacing area, the electrostatic interactions are mainly formed by aspartic and glutamic residues of AV aequorin (Asp151, Asp159, Asp161, Glu162, and Asp175) as well as arginine and lysine residues of GFP (Lys79, Arg73, Lys45, and Arg168). Also, Arg174 of AV aequorin approaches His74 of GFP. Based on the discussion above, the formation of hydrogen bonds at the interface, the good charge complementarity, and the good shape complementarity in the interface can improve the stability of AV aequorin–GFP.

3.2. The Mechanism of Energy Transfer from CTD $^-$ to CRO $^-$ in AV Aequorin–GFP. Usually, the nonradiative ET can happen through the FRET or Dexter energy transfer (DET) mechanism.^{64,65} For FRET, the ET from donor to acceptor is through Coulombic interaction,^{64,66} but for DET, the ET is through orbital overlap and electron exchange.^{65,67} Typically, the effective distance of orbital overlap and electron exchange between the donor and acceptor does not exceed 10 Å. On the other hand, Coulombic interactions can occur over much greater distances, up to 100 Å. Consequently, FRET is primarily relevant when the donor and acceptor are separated by distances ranging from 10 to 100 Å, whereas DET is primarily applicable when they are within a closer proximity of less than 10 Å.^{68,69} As shown in Figure S7, in our 200 ns MD simulation of AV aequorin–GFP, the distance between donor (CTD $^-$) and acceptor (CRO $^-$) is in the range of 30 to 35 Å. Our docking results indicate that the ET process from CTD $^-$ to CRO $^-$ should follow the FRET mechanism, which is consistent with Morise's proposition.¹²

Now, we can focus on the ET process from S_1 -CTD $^-$ to S_0 -CRO $^-$ via the FRET mechanism [S_1 (CTD $^-$) + S_0 (CRO $^-$) \rightarrow S_0 (CTD $^-$) + S_1 (CRO $^-$)] in the second stage of AV BL. The rate of FRET (k_{ET}) can be computed by formula 1. To obtain the parameters required for formula 1, it is necessary to calculate the overlap integral between the emission spectrum of S_1 -CTD $^-$ in AV aequorin and the absorption spectrum of S_0 -CRO $^-$ in GFP. Once the overlap integral is calculated, k_{ET} needs to be determined in AV aequorin–GFP. For AV BL, we first randomly chose a snapshot in the equilibrated region and

used its geometry as the initial geometry of the QM/MM optimization. The geometries of S_1 -CTD $^-$ in AV aequorin, as well as S_0 -CRO $^-$ in GFP, were optimized at the TD ω B97X-D3/def2-SVP level. The hydrogen bonding networks around S_1 -CTD $^-$ and S_0 -CRO $^-$ are drawn in Figure 3. Then, we calculated the λ_F , λ_A and TDM values of S_1 -CTD $^-$ and S_0 -CRO $^-$ at the CASPT2/ANO-RCC-VDZP level. The calculation results are shown in Table S3, and compared to the results in Tables S1–S3, the λ_F and λ_A values starting from the randomly chosen snapshot in the equilibrated region are close to the averages of the corresponding λ_F and λ_A values starting from the three different snapshots. The transitions between the S_0 and S_1 states for both CTD $^-$ and CRO $^-$ are of the $\pi-\pi^*$ type, as confirmed by their large TDM value (see Figures S3 and S4). Next, based on the CASPT2-calculated energies and TDMs, along with the DFT/TDDFT calculated vibrational frequencies at the S_0 and S_1 states, we simulated the emission spectrum of S_1 -CTD $^-$ and the absorption spectrum of S_0 -CRO $^-$ by using the TVCF formalism in the MOMAP package. It should be noted that we considered both the electronic states and the vibrational states in the simulation of the spectrum. The simulation results, presented in Figure 4, show good agreement with the experimental results (see the caption of Figure 4 for details). Moreover, the simulated spectra of CRO $^-$ in GFP by TVCF formalism exhibit a similar shoulder peak as observed in the experimental spectra (see Figure S8).^{70,71} At last, we calculated the spectral overlap (yellow region in Figure 4) integral J by formula 4 to be 1.766×10^{-4} cm.

In the equilibrated region of the 200 ns MD trajectory for AV aequorin–GFP, we selected an equilibrated structure and optimized the QM region (CTD $^-$ and CRO $^-$) on the S_1 state at the TD ω B97X-D3/def2-SVP/MM level. The calculation process of k_{ET} in AV aequorin–GFP is shown in Figure 5. The red arrows represent the TDMs ($\vec{\mu}$) of the donor and acceptor. The blue arrow indicates the distance vector r from the center of mass (yellow dots in Figure 5) of the chromophore of the donor to that of the acceptor. The distance r was estimated to be 33.60 Å. The calculated values for $\cos \theta_T$, $\cos \theta_A$, and $\cos \theta_D$ were 0.372, -0.329, and 0.738 as shown in Figure 5 (see Table S4 for calculation details). Consequently, the orientation factor κ^2 was determined to be

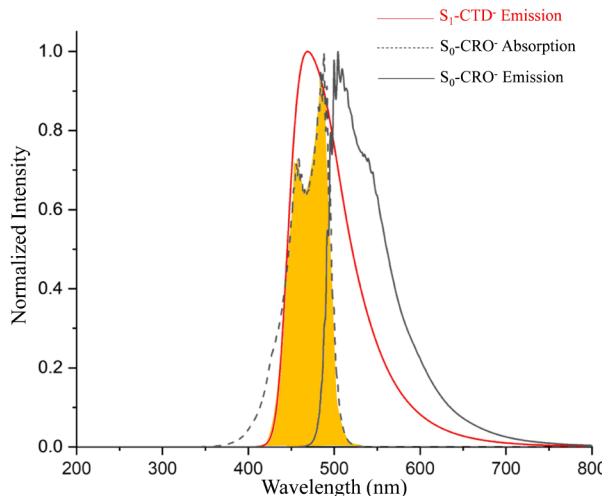


Figure 4. Simulated emission spectrum of $S_1\text{-CTD}^-$ (peak at 469 nm, exp: 470 nm)⁷² in AV aequorin, simulated absorption spectrum of $S_0\text{-CRO}^-$ (peak at 487 nm, exp: 475 nm),⁷³ and emission spectrum of $S_0\text{-CRO}^-$ (peak at 505 nm, exp: 509 nm)¹² in GFP. The yellow region represents the spectral overlap.

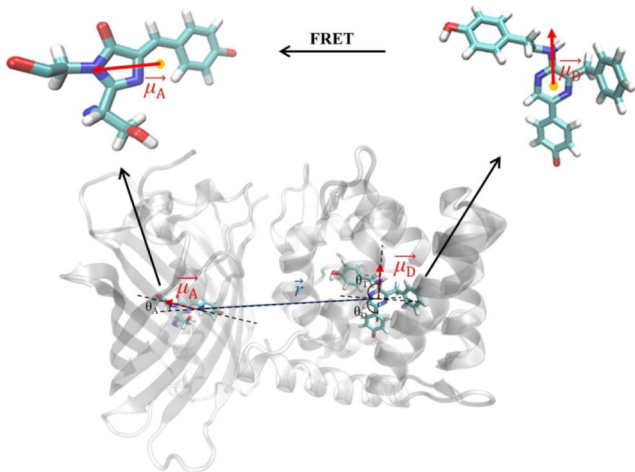


Figure 5. Optimized geometries of the CTD^- and CRO^- complex in AV aequorin–GFP at the S_1 state computed at the TD $\omega\text{B97X-D3/def2-SVP/MM}$ level. For the enlarged part on the left, the red arrow is the TDM of CRO^- ($\vec{\mu}_A$) and the yellow dot indicates the center of mass of the CRO^- chromophore. For the enlarged part on the right, the red arrow is the TDM of CTD^- ($\vec{\mu}_D$) and the yellow dot indicates the center of mass of CTD^- . The center of mass of the (yellow dots shown in the figure) donor and acceptor represent the two ends of the distance vector \vec{r} (blue arrow). θ_T , θ_A , and θ_D represent the angles between the three vectors $\vec{\mu}_A$, $\vec{\mu}_D$, and \vec{r} .

1.21 by formula 3. Based on these results, $|V_{DA}|^2$ was calculated as $7.11 \times 10^{-45} \text{ kg}^2 \text{ m}^4 \text{ s}^{-4}$. Finally, utilizing formula 1, k_{ET} was determined to be $3.77 \times 10^9 \text{ s}^{-1}$. Additionally, we selected three snapshots from the MD trajectories of AV aequorin–GFP at 160, 170, and 180 ns as the initial geometries for the QM/MM calculations and calculated the ET rate. The calculated ET rates are shown in Table S5, all of which are $\sim 10^9 \text{ s}^{-1}$.

Furthermore, we computed the fluorescence rates (k_F) and internal conversion rates (k_{IC}) of $S_1\text{-CTD}^-$ in AV aequorin, as well as $S_1\text{-CRO}^-$ in GFP, transitioning from the S_1 state to the

S_0 state using the TVCF formalism via the MOMAP package. In the studied system, the exclusive pathway for radiative decay is fluorescence. Therefore, k_F is equivalent to k_R . Due to the small SOC between the S_1 and T_1 states of CTD^- (0.02 cm^{-1} in AV aequorin) and CRO^- (0.07 cm^{-1} in GFP), computed at the CASPT2/ANO-RCC-VDZP//TD $\omega\text{B97X-D3/def2-SVP/MM}$ level, the intersystem crossing (ISC) process between the S_1 and T_1 states of CTD^- and CRO^- can be neglected. Consequently, we consider k_{IC} to be approximately equal to k_{NR} . The fluorescence quantum yield (Φ_F) was calculated using formula (7). The computational results are summarized in Table 1. The k_R and k_{NR} values of $S_1\text{-CTD}^-$ in AV aequorin

Table 1. Calculated Radiative Rate (k_R), Nonradiative Rate (k_{NR}), and Fluorescence Quantum Yield (Φ_F) of $S_1\text{-CTD}^-$ in AV Aequorin and $S_1\text{-CRO}^-$ in GFP

$S_1\text{-CTD}^-$ in AV aequorin	$S_1\text{-CRO}^-$ in GFP
$k_R (\text{s}^{-1})$	1.41×10^8
$k_{NR} (\text{s}^{-1})$	7.74×10^8
Φ_F	0.15 (0.20 ^a)
	0.98 (0.72 ^b)

^aThe fluorescence quantum yield of CTD^- in basic DMSO.²⁷ ^bThe fluorescence quantum yield of GFP.¹²

are both $\sim 10^8 \text{ s}^{-1}$. Following the introduction of GFP into the BL system of AV aequorin, the AV aequorin–GFP complex forms, facilitating the FRET process from $S_1\text{-CTD}^-$ to $S_0\text{-CRO}^-$. The calculated FRET rates are $\sim 10^9 \text{ s}^{-1}$ in AV aequorin–GFP, which are much larger than the k_R and k_{NR} of $S_1\text{-CTD}^-$. This indicates that the FRET process from $S_1\text{-CTD}^-$ to $S_0\text{-CRO}^-$ in AV aequorin–GFP occurs with high efficiency. After the efficient FRET process, $S_0\text{-CRO}^-$ is excited to $S_1\text{-CRO}^-$. As shown in Table 1, the k_{NR} of $S_1\text{-CTD}^-$ is 2 orders of magnitude higher than that of $S_1\text{-CRO}^-$. This is mainly due to the reorganization energies of CTD^- between the S_0 and the S_1 state being greater than that of CRO^- (CTD^- : 2462 cm^{-1} in AV aequorin and CRO^- : 1470 cm^{-1} in GFP). The calculated Φ_F of $S_1\text{-CRO}^-$ in GFP is 6.5 times that of $S_1\text{-CTD}^-$ in AV aequorin, which is inconsistent with the 1.2-fold enhancement in BL intensity observed experimentally.¹² This discrepancy arises because we considered only the anionic form of CRO in GFP. In reality, both neutral and anionic forms of CRO coexist in GFP, with a molar ratio of 6:1.³⁹ If we consider the molar ratio of neutral to anionic CRO, the calculated enhancement of luminescence intensity is 1.8 times, which closely matches the experimental findings and provides a reasonable explanation for the observed enhancement in BL intensity.

Based on the above discussion, the calculation results illustrated that, after the ET in AV aequorin–GFP, $S_0\text{-CRO}^-$ is excited to $S_1\text{-CRO}^-$, ultimately leading to BL. The FRET process is highly dependent on the distance and orientation between the donor and acceptor molecules, as well as the spectral overlap between the donor emission and acceptor absorption spectra. Our protein–protein docking simulations indicated a favorable interaction between AV aequorin and GFP. The QM/MM calculations confirmed that the electronic structures of CTD^- and CRO^- are conducive for FRET, with substantial overlap between the emission spectrum of $S_1\text{-CTD}^-$ and the absorption spectrum of $S_0\text{-CRO}^-$. Furthermore, since the donor and acceptor are within proteins, their relative orientation cannot be assumed as random; thus, a $\kappa^2 = 2/3$ value cannot be employed. In this study, κ^2 values are

calculated based on our actual system, which represents an advancement over traditional experimental methods.

4. CONCLUSION

AV can emit green light with a maximum emission wavelength of 509 nm under natural conditions. In addition to the regular bioluminescent system of CTD–*AV* aequorin, *AV* possesses an extra bioluminescent system, GFP. The 509 nm light is emitted by the latter system after an ET from the former system. We conducted a comprehensive investigation of the redshifted ET mechanism. We obtained *AV* aequorin–GFP structure by protein–protein docking indicating that an FRET process occurs from S₁-CTD to S₀-CRO. The FRET rates were calculated to be $\sim 10^9$ s⁻¹ through the MD simulations and QM/MM calculations, which is faster than the S₁-CTD radiative rate ($\sim 10^8$ s⁻¹) and nonradiative rate ($\sim 10^8$ s⁻¹). The rapid FRET rates indicate that the ET process from S₁-CTD to S₀-CRO in *AV* aequorin–GFP is highly efficient. The calculations of Φ_F of S₁-CRO in GFP and S₁-CTD in *AV* aequorin explain the enhancement in the BL intensity of *AV*. The understanding of the ET mechanism in the *AV* system not only explains the energy source of GFP but also helps to understand other bioluminescent systems and provides new insights into the BRET technique.

■ ASSOCIATED CONTENT

Supporting Information

The Supporting Information is available free of charge at <https://pubs.acs.org/doi/10.1021/acs.jpcb.4c08330>.

The details in calculation methods; the RMS deviation in MD simulation; the 16-in-14 and 14-in-13 active space orbitals used in CASPT2 calculations; the simulated and experimental spectrum of CRO[−] and CTD[−]; the information on *AV* aequorin–GFP complex; the vertical absorption wavelength, vertical emission wavelength, and oscillator strength of CRO[−] and CTD[−] and details in calculating the orientation factor, κ^2 ([PDF](#))

■ AUTHOR INFORMATION

Corresponding Authors

Deping Hu – Department of Chemistry, Faculty of Arts and Sciences, Center for Advanced Materials Research, Beijing Normal University, Zhuhai 519087, China;  orcid.org/0000-0001-7161-1253; Email: depinghu@bnu.edu.cn

Ya-Jun Liu – Department of Chemistry, Faculty of Arts and Sciences, Center for Advanced Materials Research, Beijing Normal University, Zhuhai 519087, China; Key Laboratory of Theoretical and Computational Photochemistry, Ministry of Education, College of Chemistry, Beijing Normal University, Beijing 100875, China;  orcid.org/0000-0001-8761-5339; Email: yajun.liu@bnu.edu.cn

Author

Shuangqi Pi – Department of Chemistry, Faculty of Arts and Sciences, Center for Advanced Materials Research, Beijing Normal University, Zhuhai 519087, China

Complete contact information is available at:

<https://pubs.acs.org/10.1021/acs.jpcb.4c08330>

Notes

The authors declare no competing financial interest.

■ ACKNOWLEDGMENTS

This work was supported by grants from the National Natural Science Foundation of China (Grant Nos. 22373010, 21973005, and 22403008) and the Beijing Natural Science Foundation (Grant No. 2244074). Computing resources were provided by the Interdisciplinary Intelligence Super Computer Center of Beijing Normal University at Zhuhai.

■ REFERENCES

- (1) Day, R. N.; Davidson, M. W. The fluorescent protein palette: tools for cellular imaging. *Chem. Soc. Rev.* **2009**, *38* (10), 2887–2921.
- (2) Zimmer, M. GFP: from jellyfish to the Nobel prize and beyond. *Chem. Soc. Rev.* **2009**, *38* (10), 2823–2832.
- (3) Ward, R. E.; Reid, P.; Bashirullah, A.; D'Avino, P. P.; Thummel, C. S. GFP in living animals reveals dynamic developmental responses to ecdysone during drosophila metamorphosis. *Dev. Biol.* **2003**, *256* (2), 389–402.
- (4) Wan, H.; Korzh, S.; Li, Z.; Mudumana, S. P.; Korzh, V.; Jiang, Y.-J.; Lin, S.; Gong, Z. Analyses of pancreas development by generation of gfp transgenic zebrafish using an exocrine pancreas-specific elastaseA gene promoter. *Exp. Cell Res.* **2006**, *312* (9), 1526–1539.
- (5) Steel, E.; Barker, I.; Danks, C.; Coates, D.; Boonham, N. A. tumefaciens-mediated transient expression as a tool for antigen production for cucurbit yellow stunting disorder virus. *J. Virol. Methods* **2010**, *163* (2), 222–228.
- (6) Yin, H.; Ye, X.; Li, Y.; Niu, Q.; Wang, C.; Ma, W. Evaluation of the effects of systemic photodynamic therapy in a rat model of acute myeloid leukemia. *J. Photochem. Photobiol. B: Biol.* **2015**, *153*, 13–19.
- (7) Miyawaki, A.; Llopis, J.; Heim, R.; McCaffery, J. M.; Adams, J. A.; Ikura, M.; Tsien, R. Y. Fluorescent indicators for Ca²⁺-based on green fluorescent proteins and calmodulin. *Nature* **1997**, *388* (6645), 882–887.
- (8) Shimomura, O.; Johnson, F. H.; Saiga, Y. Extraction, Purification and Properties of Aequorin, a Bioluminescent Protein from the Luminous Hydromedusan, Aequorea. *J. Cell. Comp. Physiol.* **1962**, *59* (3), 223–239.
- (9) Shimomura, O. Bioluminescence in the sea: Photoprotein systems. *Symp. Soc. Exp. Biol.* **1985**, *39*, 351–372.
- (10) Shimomura, O.; Johnson, F. H.; Morise, H. Mechanism of the luminescent intramolecular reaction of aequorin. *Biochemistry* **1974**, *13* (16), 3278–3286.
- (11) Morin, J. G.; Hastings, J. W. Energy transfer in a bioluminescent system. *J. Cell. Physiol.* **1971**, *77* (3), 313–318.
- (12) Morise, H.; Shimomura, O.; Johnson, F. H.; Winant, J. Intermolecular energy transfer in the bioluminescent system of Aequorea. *Biochemistry* **1974**, *13* (12), 2656–2662.
- (13) Grigorenko, B. L.; Krylov, A. I.; Nemukhin, A. V. Molecular Modeling Clarifies the Mechanism of Chromophore Maturation in the Green Fluorescent Protein. *J. Am. Chem. Soc.* **2017**, *139* (30), 10239–10249.
- (14) Cody, C. W.; Prasher, D. C.; Westler, W. M.; Prendergast, F. G.; Ward, W. W. Chemical structure of the hexapeptide chromophore of the Aequorea green-fluorescent protein. *Biochemistry* **1993**, *32* (5), 1212–1218.
- (15) Shimomura, O. Structure of the chromophore of Aequorea green fluorescent protein. *FEBS Lett.* **1979**, *104* (2), 220–222.
- (16) van Thor, J. J. Photoreactions and dynamics of the green fluorescent protein. *Chem. Soc. Rev.* **2009**, *38* (10), 2935–2950.
- (17) Donati, G.; Petrone, A.; Caruso, P.; Rega, N. The mechanism of a green fluorescent protein proton shuttle unveiled in the time-resolved frequency domain by excited state ab initio dynamics. *Chem. Sci.* **2018**, *9* (5), 1126–1135.
- (18) Reuter, N.; Lin, H.; Thiel, W. Green Fluorescent Proteins: Empirical Force Field for the Neutral and Deprotonated Forms of the Chromophore. Molecular Dynamics Simulations of the Wild Type and S65T Mutant. *J. Phys. Chem. B* **2002**, *106* (24), 6310–6321.

- (19) Heim, R.; Prasher, D. C.; Tsien, R. Y. Wavelength mutations and posttranslational autoxidation of green fluorescent protein. *Proc. Natl. Acad. Sci. U. S. A.* **1994**, *91* (26), 12501–12504.
- (20) Ormö, M.; Cubitt, A. B.; Kallio, K.; Gross, L. A.; Tsien, R. Y.; Remington, S. J. Crystal Structure of the *Aequorea victoria* Green Fluorescent Protein. *Science* **1996**, *273* (5280), 1392–1395.
- (21) Heim, R.; Tsien, R. Y. Engineering green fluorescent protein for improved brightness, longer wavelengths and fluorescence resonance energy transfer. *Curr. Biol.* **1996**, *6* (2), 178–182.
- (22) Ausili, A.; Staiano, M.; Marabotti, A.; D'Auria, G.; Gómez-Fernández, J. C.; Torrecillas, A.; Ortiz, A.; D'Auria, S. Correlation between fluorescence and structure in the orange-emitting GFP-like protein, monomeric Kusabira Orange. *J. Photochem. Photobiol. B Biol.* **2014**, *138*, 223–229.
- (23) Chen, S.-F.; Navizet, I.; Roca-Sanjuán, D.; Lindh, R.; Liu, Y.-J.; Ferré, N. Chemiluminescence of Coelenterazine and Fluorescence of Coelenteramide: A Systematic Theoretical Study. *J. Chem. Theory Comput.* **2012**, *8* (8), 2796–2807.
- (24) van Oort, B.; Eremeeva, E. V.; Koehorst, R. B. M.; Laptenok, S. P.; van Amerongen, H.; van Berkel, W. J. H.; Malikova, N. P.; Markova, S. V.; Vysotski, E. S.; Visser, A. J. W. G. Picosecond Fluorescence Relaxation Spectroscopy of the Calcium-Discharged Photoproteins Aequorin and Obelin. *Biochemistry* **2009**, *48* (44), 10486–10491.
- (25) Yue, L. QM/MM Investigations on the Bioluminescent Decomposition of Coelenterazine Dioxetanone in Obelin. *Chem. Res. Chin. Univ.* **2018**, *34* (5), 758–766.
- (26) Lee, J. W. *Bioluminescence, the nature of the light*; University of Georgia Libraries: Athens, GA, 2017.
- (27) Imai, Y.; Shibata, T.; Maki, S.; Niwa, H.; Ohashi, M.; Hirano, T. Fluorescence properties of phenolate anions of coelenteramide analogues: the light-emitter structure in aequorin bioluminescence. *J. Photochem. Photobiol., A* **2001**, *146* (1), 95–107.
- (28) Kobayashi, H.; Picard, L.-P.; Schönenegg, A.-M.; Bouvier, M. Bioluminescence resonance energy transfer-based imaging of protein–protein interactions in living cells. *Nat. Protoc.* **2019**, *14* (4), 1084–1107.
- (29) Tsuboi, S.; Jin, T. BRET based dual-colour (visible/near-infrared) molecular imaging using a quantum dot/EGFP–luciferase conjugate. *RSC Adv.* **2019**, *9* (60), 34964–34971.
- (30) Wu, C.; Mino, K.; Akimoto, H.; Kawabata, M.; Nakamura, K.; Ozaki, M.; Ohmiya, Y. In vivo far-red luminescence imaging of a biomarker based on BRET from Cypridina bioluminescence to an organic dye. *Proc. Natl. Acad. Sci. U. S. A.* **2009**, *106* (37), 15599–15603.
- (31) König, C.; Neugebauer, J. Quantum Chemical Description of Absorption Properties and Excited-State Processes in Photosynthetic Systems. *ChemPhysChem* **2012**, *13* (2), 386–425.
- (32) Sun, Y.; Giebink, N. C.; Kanno, H.; Ma, B.; Thompson, M. E.; Forrest, S. R. Management of singlet and triplet excitons for efficient white organic light-emitting devices. *Nature* **2006**, *440* (7086), 908–912.
- (33) Head, J. F.; Inouye, S.; Teranishi, K.; Shimomura, O. The crystal structure of the photoprotein aequorin at 2.3 Å resolution. *Nature* **2000**, *405* (6784), 372–376.
- (34) Mori, K.; Maki, S.; Niwa, H.; Ikeda, H.; Hirano, T. Real light emitter in the bioluminescence of the calcium-activated photoproteins aequorin and obelin: light emission from the singlet-excited state of coelenteramide phenolate anion in a contact ion pair. *Tetrahedron* **2006**, *62* (26), 6272–6288.
- (35) Chen, S.-F.; Ferré, N.; Liu, Y.-J. QM/MM Study on the Light Emitters of Aequorin Chemiluminescence, Bioluminescence, and Fluorescence: A General Understanding of the Bioluminescence of Several Marine Organisms. *Chem.-Eur. J.* **2013**, *19* (26), 8466–8472.
- (36) Bravaya, K. B.; Khrenova, M. G.; Grigorenko, B. L.; Nemukhin, A. V.; Krylov, A. I. Effect of Protein Environment on Electronically Excited and Ionized States of the Green Fluorescent Protein Chromophore. *J. Phys. Chem. B* **2011**, *115* (25), 8296–8303.
- (37) Sinicropi, A.; Andruniow, T.; Ferré, N.; Basosi, R.; Olivucci, M. Properties of the Emitting State of the Green Fluorescent Protein Resolved at the CASPT2//CASSCF/CHARMM Level. *J. Am. Chem. Soc.* **2005**, *127* (33), 11534–11535.
- (38) Brejc, K.; Sixma, T. K.; Kitts, P. A.; Kain, S. R.; Tsien, R. Y.; Ormö, M.; Remington, S. J. Structural basis for dual excitation and photoisomerization of the *Aequorea victoria* green fluorescent protein. *Proc. Natl. Acad. Sci. U. S. A.* **1997**, *94* (6), 2306–2311.
- (39) Chatteraj, M.; King, B. A.; Bublitz, G. U.; Boxer, S. G. Ultra-fast excited state dynamics in green fluorescent protein: multiple states and proton transfer. *Proc. Natl. Acad. Sci. U. S. A.* **1996**, *93* (16), 8362–8367.
- (40) Yang, F.; Moss, L. G.; Phillips, G. N. The molecular structure of green fluorescent protein. *Nat. Biotechnol.* **1996**, *14* (10), 1246–1251.
- (41) Desta, I. T.; Porter, K. A.; Xia, B.; Kozakov, D.; Vajda, S. Performance and Its Limits in Rigid Body Protein-Protein Docking. *Structure* **2020**, *28* (9), 1071–1081.
- (42) Kozakov, D.; Hall, D. R.; Xia, B.; Porter, K. A.; Padhorny, D.; Yueh, C.; Beglov, D.; Vajda, S. The ClusPro web server for protein–protein docking. *Nat. Protoc.* **2017**, *12* (2), 255–278.
- (43) Jorgensen, W. L.; Chandrasekhar, J.; Madura, J. D.; Impey, R. W.; Klein, M. L. Comparison of simple potential functions for simulating liquid water. *J. Chem. Phys.* **1983**, *79* (2), 926–935.
- (44) Case, D. A.; Betz, R. M.; Cerutti, D. S.; Cheatham, T. E., III; Darden, T. A.; Duke, R. E.; Giese, T. J.; Gohlke, H.; Götz, A. W.; Homeyer, N., et al. *Amber 16*; University of California: San Francisco, 2016.
- (45) Weigend, F.; Ahlrichs, R. Balanced basis sets of split valence, triple zeta valence and quadruple zeta valence quality for H to Rn: Design and assessment of accuracy. *Phys. Chem. Chem. Phys.* **2005**, *7* (18), 3297–3305.
- (46) Lin, Y.-S.; Li, G.-D.; Mao, S.-P.; Chai, J.-D. Long-Range Corrected Hybrid Density Functionals with Improved Dispersion Corrections. *J. Chem. Theory Comput.* **2013**, *9* (1), 263–272.
- (47) Kästner, J.; Carr, J. M.; Keal, T. W.; Thiel, W.; Wander, A.; Sherwood, P. DL-FIND: An Open-Source Geometry Optimizer for Atomistic Simulations. *J. Phys. Chem. A* **2009**, *113* (43), 11856–11865.
- (48) Sherwood, P.; de Vries, A. H.; Guest, M. F.; Schreckenbach, G.; Catlow, C. R. A.; French, S. A.; Sokol, A. A.; Bromley, S. T.; Thiel, W.; Turner, A. J. QUASI: A general purpose implementation of the QM/MM approach and its application to problems in catalysis. *J. Mol. Struct.: THEOCHEM* **2003**, *632* (1), 1–28.
- (49) Metz, S.; Kästner, J.; Sokol, A. A.; Keal, T. W.; Sherwood, P. ChemShell—a modular software package for QM/MM simulations. *Wiley Interdiscip. Rev.: comput. Mol. Sci.* **2014**, *4* (2), 101–110.
- (50) Neese, F. Software update: The ORCA program system—Version 5.0. *Wiley Interdiscip. Rev.: comput. Mol. Sci.* **2022**, *12* (5), No. e1606.
- (51) Smith, W.; Forester, T. R. DL_Poly_2.0: A general-purpose parallel molecular dynamics simulation package. *J. Mol. Graphics* **1996**, *14* (3), 136–141.
- (52) Andersson, K.; Malmqvist, P. Å.; Roos, B. O. Second-order perturbation theory with a complete active space self-consistent field reference function. *J. Chem. Phys.* **1992**, *96* (2), 1218–1226.
- (53) Aquilante, F.; Autschbach, J.; Carlson, R. K.; Chibotaru, L. F.; Delcey, M. G.; De Vico, L.; Fdez. Galván, I.; Ferré, N.; Frutos, L. M.; Gagliardi, L.; et al. Molcas 8: New capabilities for multiconfigurational quantum chemical calculations across the periodic table. *J. Comput. Chem.* **2016**, *37* (5), 506–541.
- (54) Ferré, N.; Ángyan, J. G. Approximate electrostatic interaction operator for QM/MM calculations. *Chem. Phys. Lett.* **2002**, *356* (3), 331–339.
- (55) Arbelo-González, W.; Crespo-Otero, R.; Barbatti, M. Steady and Time-Resolved Photoelectron Spectra Based on Nuclear Ensembles. *J. Chem. Theory Comput.* **2016**, *12* (10), 5037–5049.
- (56) Knox, R. S.; van Amerongen, H. Refractive Index Dependence of the Förster Resonance Excitation Transfer Rate. *J. Phys. Chem. B* **2002**, *106* (20), 5289–5293.

- (57) McMeekin, T. L.; Wilensky, M.; Groves, M. L. Refractive indices of proteins in relation to amino acid composition and specific volume. *Biochem. Biophys. Res. Commun.* **1962**, *7* (2), 151–156.
- (58) Toptygin, D.; Savtchenko, R. S.; Meadow, N. D.; Roseman, S.; Brand, L. Effect of the Solvent Refractive Index on the Excited-State Lifetime of a Single Tryptophan Residue in a Protein. *J. Phys. Chem. B* **2002**, *106* (14), 3724–3734.
- (59) Niu, Y.; Li, W.; Peng, Q.; Geng, H.; Yi, Y.; Wang, L.; Nan, G.; Wang, D.; Shuai, Z. J. M. P. MOlecular MAterials Property Prediction Package (MOMAP) 1.0: a software package for predicting the luminescent properties and mobility of organic functional materials. *Mol. Phys.* **2018**, *116* (7–8), 1078–1090.
- (60) Shuai, Z. Thermal Vibration Correlation Function Formalism for Molecular Excited State Decay Rates. *Chin. J. Chem.* **2020**, *38* (11), 1223–1232.
- (61) Shuai, Z.; Peng, Q. Excited states structure and processes: Understanding organic light-emitting diodes at the molecular level. *Phys. Rep.* **2014**, *S37* (4), 123–156.
- (62) Shuai, Z.; Peng, Q. Organic light-emitting diodes: theoretical understanding of highly efficient materials and development of computational methodology. *Natl. Sci. Rev.* **2017**, *4* (2), 224–239.
- (63) Conte, L. L.; Chothia, C.; Janin, J. The atomic structure of protein-protein recognition sites. *J. Mol. Biol.* **1999**, *285* (5), 2177–2198.
- (64) Förster, T. 10th Spiers Memorial Lecture. Transfer mechanisms of electronic excitation. *Discuss. Faraday Soc.* **1959**, *27*, 7–17.
- (65) Dexter, D. L. A Theory of Sensitized Luminescence in Solids. *J. Chem. Phys.* **1953**, *21* (5), 836–850.
- (66) You, Z.-Q.; Hsu, C.-P. Theory and calculation for the electronic coupling in excitation energy transfer. *Int. J. Quantum Chem.* **2014**, *114* (2), 102–115.
- (67) Bai, S.; Zhang, P.; Beratan, D. N. Predicting Dexter Energy Transfer Interactions from Molecular Orbital Overlaps. *J. Phys. Chem. C* **2020**, *124* (35), 18956–18960.
- (68) Han, J.; Chen, X.; Shen, L.; Chen, Y.; Fang, W. H.; Wang, H. Energy Transfer Tunes Phosphorescent Color of Single-Dopant White OLEDs. *Chem.-Eur. J.* **2011**, *17* (50), 13971–13977.
- (69) Sapsford, K. E.; Berti, L.; Medintz, I. L. Materials for Fluorescence Resonance Energy Transfer Analysis: Beyond Traditional Donor–Acceptor Combinations. *Angew. Chem., Int. Ed.* **2006**, *45* (28), 4562–4589.
- (70) Creemers, T. M. H.; Lock, A. J.; Subramaniam, V.; Jovin, T. M.; Völker, S. Three photoconvertible forms of green fluorescent protein identified by spectral hole-burning. *Nat. Struct. Biol.* **1999**, *6* (6), 557–560.
- (71) Cormier, M. J.; Hori, K.; Karkhanis, Y. D.; Anderson, J. M.; Wampler, J. E.; Morin, J. G.; Hastings, J. W. Evidence for similar biochemical requirements for bioluminescence among the coelenterates. *J. Cell. Physiol.* **1973**, *81* (2), 291–297.
- (72) Shimomura, O.; Johnson, F. H. Calcium Binding, Quantum Yield, and Emitting Molecule in Aequorin Bioluminescence. *Nature* **1970**, *227* (5265), 1356–1357.
- (73) Elsliger, M.-A.; Wachter, R. M.; Hanson, G. T.; Kallio, K.; Remington, S. J. Structural and Spectral Response of Green Fluorescent Protein Variants to Changes in pH. *Biochemistry* **1999**, *38* (17), 5296–5301.